

## An effective thickness proposal for strength evaluation of one-side pitted steel plates under uniaxial compression

### Abstract

This paper presents the results of an investigation into the post-buckling behaviour and ultimate strength of imperfect pitted steel plates used in ship and other marine-related structures. A series of elastic-plastic large deflection finite element analyses is performed on pitted steel plates. The effects of pitting corrosion on one side of the plates are introduced into the finite element models. The effects on plate compressive strength as a result of parametric variation of the pitting corrosion geometry are evaluated. A proposal on the effective thickness is concluded in order to estimate the ultimate strength and explore the post-buckling behaviour of pitted steel plates under uniaxial compression.

### Keywords

steel plate, pitting corrosion, uniaxial compression, effective thickness

Zorareh Hadj Mohammad  
Esmail Nouri<sup>a</sup> and Mohammad  
Reza Khedmati<sup>b,\*</sup> and Shokoufeh Sadeghifard<sup>c</sup>

<sup>a</sup>Department of Marine Technology, Amirkabir University of Technology, Tehran 15914, Iran

<sup>b</sup>Department of Marine Technology, Amirkabir University of Technology, Tehran 15914, Iran

<sup>c</sup>Department of Marine Technology, Amirkabir University of Technology, Tehran 15914, Iran

Received 17 Apr 2012;  
In revised form 27 Apr 2012

\* Author email: [khedmati@aut.ac.ir](mailto:khedmati@aut.ac.ir)

## 1 INTRODUCTION

Corrosion in marine structures is mainly observed in two distinct types, namely, general corrosion and pitting corrosion. General corrosion is the problem when the plate elements such as the hold frames of bulk carriers have no protective coating. Both surfaces of the plate may be corroded, in a pattern like the sea waves spectrum. Generally, pitting corrosion is defined as an extremely localised corrosive attack and sites of the corrosive attack are relatively small compared to the overall exposed surface [1].

Pitting occurs on the ship's steel structures that are in contact with water (such as the bottom and side shell plating) or subject to wind and water conditions (such as the boot topping area) as well as in the tanks carrying liquid cargoes or ballast. Excessively deep pits can lead to perforation of the plate and possibly to serious pollution. Pitting does not occur in areas of plating that are not immersed in water and/or subject only to spray. Pitting corrosion of hold frames in way of cargo holds of bulk carriers which have coating such as tar epoxy paints is also reported and studied by Nakai et al.[15].

In the case of localised corrosion observed on hold frames of bulk carriers, the sites of the corrosive attack, that is, pits are relatively large (up to about 50 mm in diameter).

## NOTATIONS

$\alpha$	Plate length
$A$	Area
$AR$	Aspect ratio of the plate
$A_{0mm}$	Coefficients in initial deflection function
$A_{pit}$	Pit area $\left( = \frac{\pi D_{pit}^2}{4} \right)$
$b$	Plate width
$D$	Diameter
$DOP$	Density of pitting $\left( = \frac{n_{pit} A_{pit}}{ab} \right)$ 2
$d_w$	Uniform reduction in thickness
$E$	Young modulus of material
$H$	Pit depth
$m$	Number of half-waves in longitudinal direction
$n$	Number of half-waves in transverse direction
$n_{pit}$	Number of pit(s)
$n_y$	Number of years of exposure
$r_1, r_2$	Random numbers corresponding to the corroded surfaces of the plate
$RDP$	Ratio of pit diameter to depth of pit $\left( = \frac{D_{pit}}{H} \right)$ 3
$S$	Standard deviation of random thickness variations
$t(=t_0)$	Thickness of plate in uncorroded condition
$t_{avg}$	Average thickness $\left( = \frac{V_{uncorroded} - V_{corroded}}{A} \right)$ 4
$t_{eq}$	Effective thickness
$t_n$	Equivalent uniform thickness of the corroded plate, after $n$ years of exposure
$tp$	Thickness function in general corrosion model
$U_x$	Displacement along X-axis
$U_y$	Displacement along Y-axis
$U_z$	Displacement along Z-axis
$V$	Volume
$V_{corroded}$	Volume of the pits $(= n_{pit} \cdot V_{pit})$ 5
$V_{pit}$	Volume of one pit $\left( = \frac{1}{3} A_{pit} \frac{1}{D_{pit} \cdot RDP} \right)$ 6
$W$	Original weight of uncorroded plate
$W_0$	Initial deflection function
$W_{0max}$	Maximum magnitude of initial deflection
$W_n$	Actual weight of the corroded plate after $n$ years of exposure
$Z_{UPSRF}$	Z-coordinate of the upper surface of the plate
$Z_{LowSRF}$	Z-coordinate of the lower surface of the plate
$\nu$	Poisson's ratio of material
$\alpha$	Coefficient describing different parameters of the pitted plate
$\beta$	Plate slenderness parameter $\left( = \frac{b}{t} \sqrt{\frac{\sigma_Y}{E}} \right)$ 7
$m$	Equivalent mean corrosion depth of the pitted plate
$\rho$	Density of plate material
$\epsilon$	Strain
$\epsilon_y$	Material yield strain $(= \sigma_Y/E)$ 8
$\sigma$	Stress
$\sigma_{Final}$	Final strength
$\sigma_Y$	Material yield stress
$\sigma_U$	Material ultimate stress
$\sigma_{cr}$	Buckling strength of the plate
$\sigma_{Ult}$	Ultimate strength of the plate

## 2 RESEARCH BACKGROUND ON THE STRENGTH OF CORRODED ELEMENTS

The problem of strength analysis of plates and stiffened plates incorporating different corrosion types has attracted the attention of some researchers. Daidola et al. [4] proposed a mathematical model to estimate the residual thickness of pitted plates using the average and maximum values of pitting data or the number of pits and the depth of the deepest pit, and presented a method to assess the effect of thickness reduction due to pitting on local yielding and plate buckling based on the probabilistic approach. Furthermore, they developed a set of tools which can be used to assess the residual strength of pitted plates. Paik et al.[19, 20] studied the ultimate strength characteristics of pitted plate elements under axial compressive loads and in-plane shear loads, and derived closed form formulae for predicting the ultimate strength of pitted plates using the strength reduction (knock-down) factor approach. They dealt with the case where the shape of corrosion pits is a cylinder. Dunbar et al. [22] investigated the effects of localised corrosion on the strength of plates and stiffened plates. They applied finite element analyses in order to study initial buckling, ultimate collapse and post-ultimate responses of the corroded plates and stiffened plates. Nakai and his collaborators[15, 16] performed a series of nonlinear finite-element (FE) analyses with pitted plates and stiffened plates subjected to in-plane compressive loads and bending moments in order to investigate their behaviours. They also established a method for prediction of ultimate strength of plate and stiffened plate models with pitted corrosion. Ok et al.[18] focused on assessing the effects of localised pitting corrosion which concentrates at one or several possibly large area on the ultimate strength of unstiffened plates. They applied multi-variable regression method to derive new formulae to predict ultimate strength of unstiffened plates with localised corrosion. Their results indicated that the length, width and depth of pit corrosion have weakening effects on the ultimate strength of the plates while plate slenderness has only marginal effect on strength reduction. It was also revealed by them that transverse location of pit corrosion is an important factor determining the amount of strength reduction. Zhang et al.[27] focused on the development of an assessing method for ultimate strength of ship hull plate with corrosion damage. Pitting corrosion results in a quantity loss of the plate material as well as a significant degradation of the ultimate strength of the hull plate due to reducing of the effective thickness of the plate. Accordingly, the model for describing the correlations between the ultimate strength and the corroded volume loss of a corroded plate was proposed by them based on relative theory. Such model was then completed through numerical experiment by nonlinear finite element analyses for series of corroded plate models. Later Saad Eldeen and Guedes Soares[5] investigated the collapse strength of pitted plates under in-plane compression. They performed some non-linear finite element analyses on the plates with different corrosion densities. Based on the obtained results, they could derive a formula in order to predict the ultimate strength reduction for the plates with pitting corrosion. Also Jiang and Guedes Soares [10] studied the ultimate strength of steel plates with single and double side corrosion pits. Huang et al. [9] extended their formulation in order to predict the ultimate strength of pitted square plates under biaxial compression. Besides, Amlashi and Moan [3] assessed the strength behaviour of stiffened plates suffering pitting corrosion under bi-axial compressive loading. They reached

the conclusion that the most important parameters influencing the ultimate strength of the pitted stiffened plates under bi-axial compressive loads are the smallest sectional area and also density of pitting.

There have been also some research works on the strength of plates and stiffened plates suffering general corrosion. Mateus and Witz [14] investigated the effect of general corrosion on the post-buckling of plates using the uniform thickness reduction approach and a quasi-random thickness surface model. They revealed that the usual uniform thickness reduction approach to account for general corrosion effects is not adequate because plastic hinges formed due to plate surface irregularity slightly decreases its ultimate strength and significantly affects the post buckling behaviour of the plate. Teixeira and Guedes Soares [8, 23, 24] investigated the collapse behaviour and ultimate strength of plates with random spatial distributions of corroded thicknesses. They demonstrated the importance of the spatial representation of the corrosion by random fields as an alternative to the traditional approach, based on a uniform reduction of the plate thickness. Seo et al. [21] validated the equivalent plate thickness approach for ultimate strength analysis of stiffened panels with non-uniform plate thickness. Khedmati et al. [13] made an extensive numerical study on the strength of steel plates with both-sides randomly distributed with corrosion wastage under uniaxial compression. They also proposed an effective thickness formulation for strength assessment of these plates under uniaxial compression [12]. Nouri et al. [17] studied numerically the strength and collapse behaviour of stiffened plates with both-sides randomly distributed with corrosion wastage under uniaxial compression.

The main objective of the present paper is to propose a formulation in order to give the effective thickness for strength assessment of the pitted plates under uniaxial compression. The pitting corrosion is considered to be distributed over the surfaces of the plate. In order to achieve this goal, first, different aspects of finite element modelling for the pitted plates are established in the Section 3 considering their application in the marine structures. The established finite element model is unique, since it incorporates initial imperfections as can be observed in real practice. A special methodology is adopted in creating the pits inside the finite element plate models. Post-buckling behaviour and ultimate strength of imperfect pitted steel plates are investigated applying elastic-plastic large deflection finite element analysis, the results of which are described in the Section 4. The effects on plate compressive strength as a result of parametric variation of the pitting corrosion geometry are evaluated. Finally, based on the gathered database, in Section 5 a proposal on the effective thickness is concluded in order to estimate the ultimate strength and explore the post-buckling behaviour of pitted steel plates under uniaxial compression. The derived proposal can be easily implemented in the strength evaluation of plated structures suffering the pitting corrosion.

### 3 FINITE ELEMENT ANALYSIS (FEA)

#### 3.1 Extent of the model

The plates in ships and offshore structures are continuous. Longitudinal stiffeners and transverse frames divide the surface of the plates into isolated regions, Fig. 1(a). Such regions, which are shaded in Fig. 1(a), are considered as the model extent in the analyses.

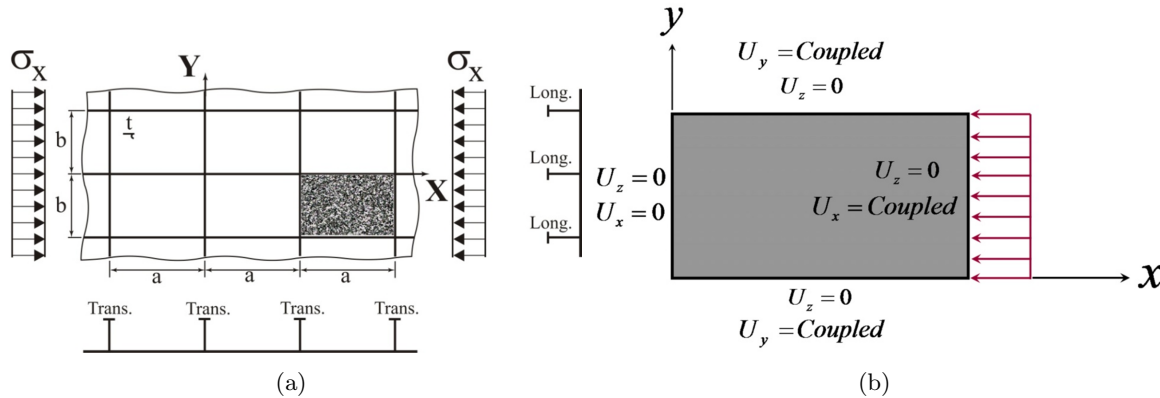


Figure 1 (a) Extent of the model, (b) Boundary and loading conditions.

#### 3.2 Loading and boundary conditions

As shown in Fig. 1(a), the plate is in fact of continuous nature. The continuous plate is divided into a number of local plate panels surrounded by longitudinal stiffeners and transverse frames. To consider the effects of longitudinal stiffeners and transverse frames in the behaviour of local plate panel model, proper boundary conditions are to be applied on it. The boundary conditions were common to all cases and represented those typically found in marine structures, Fig. 1(b).

Out-of-plane movement was restrained for all plate edges. The loaded edges (the two transverse edges) were kept straight mainly due to the continuity of plate and partly owing to the presence of stiff transverse frames. This has been demonstrated in the Fig. 1(b) with imposing " $U_x=0$ " or " $U_x=\text{Coupled}$ " condition on the nodes lying on the transverse edges of the finite element model. Because the plate is a part of a continuous panel, the unloaded edges are not entirely free to move in their own plane after buckling. The commonly used assumption that the edges are kept straight, but otherwise free to move in plane direction, were adopted in the analyses. To prevent rigid body motion, minimum boundary conditions were applied in the x and y directions. No rotational restraints were applied. Loading would be compressive along x-axis of the Fig. 1(b). The uniaxial compressive loading was applied by controlled edge displacement.

### 3.3 Finite Element code, adopted element, mesh density and nonlinear parameters

The ANSYS version 11.0 was used in all FE analyses. A code was prepared in APDL (ANSYS Parametric Design Language) to facilitate the parametric modelling and analysis using ANSYS [2].

Plates are modelled by SHELL181 elements with elastic-plastic large deflection solution option. SHELL181 is suitable for analyzing thin to moderately-thick shell structures. It is a 4-node element with six degrees of freedom at each node: translations in the x, y, and z directions, and rotations about the x, y, and z-axes. SHELL181 is well-suited for linear, large rotation, and/or large strain nonlinear applications. Changes in shell thickness are accounted for in nonlinear analyses. In order to obtain reasonable results, a number of sensitivity analyses were carried out to find out the optimum mesh density and proper values of nonlinear analysis options. It was found that 40 longitudinal divisions and 20 transversal divisions are enough in order to discretise the plate. A more accurate discretisation with a refinement order of 9 was used to model the pits. Arc-length nonlinear method has been used to obtain loading and unloading patterns of the plates under compression.

A sample finite element discretisation for a plate with cone type pitting corrosion is represented in Fig. 2. Each of the pits has a depth of  $H_{pit}$  and a base diameter of  $D_{pit}$ . The number of pits is  $n_{pit}$ . Other geometric characteristics of the pits are pit area ( $A_{pit}$ ), density of pitting ( $DOP$ ), ratio of pit diameter to the depth of the pit ( $RDP$ ) and the volume of the pit ( $V_{pit}$ ). The prepared code finds the position of the pits according to a rational procedure and based on the chosen density of pitting ( $DOP$ ). First of all, the code calculates area of each pit and finds number of total required pits to meet desired  $DOP$ . Then, the pits are generated in a systematic way considering their assumed dimensions and uniform distribution in length and width of plate.

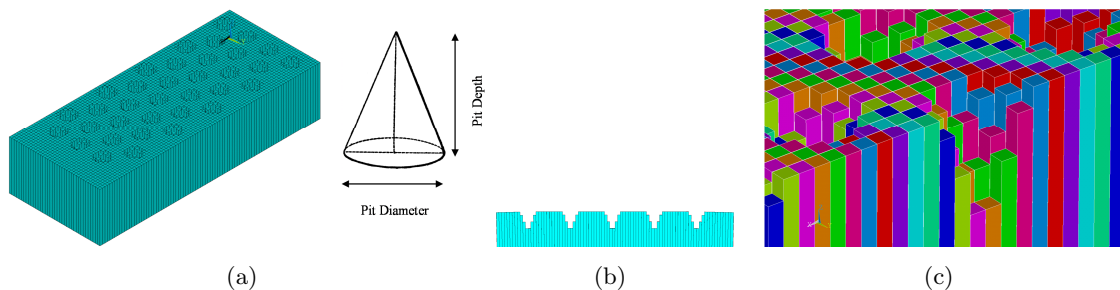


Figure 2 (a) Scaled views of the Finite element discretisation of the pitted plate, (b) Magnified cross-sectional view of the pitted plate, (c) Zoomed view of the pitted plate.

### 3.4 Applied material properties

The material used in the parametric models was of two different types: normal strength steel (abbreviated by NS steel) and high tensile strength steel (abbreviated by HTS steel). Both types of steels have a Young's modulus of 205.8  $GPa$  and a Poisson's ratio of 0.3. The yield strength

of 235.2 MPa and 362.6 MPa are respectively taken into account for NS and HTS steels. It is evident that strain-hardening effect has some influence on the nonlinear behaviour of plates. The degree of such an influence is a function of many factors including plate slenderness. In this study, material behaviour for plate was modelled in a bi-linear elastic-plastic manner with strain-hardening rate of  $E/65$ , Fig. 3. This value of strain-hardening rate was obtained through a large number of elastic-plastic large deflection analyses made by Khedmati [11].

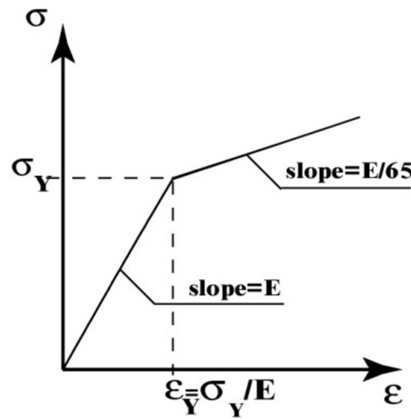


Figure 3 Idealised bilinear model of stress-strain curve for material.

### 3.5 Initial imperfections

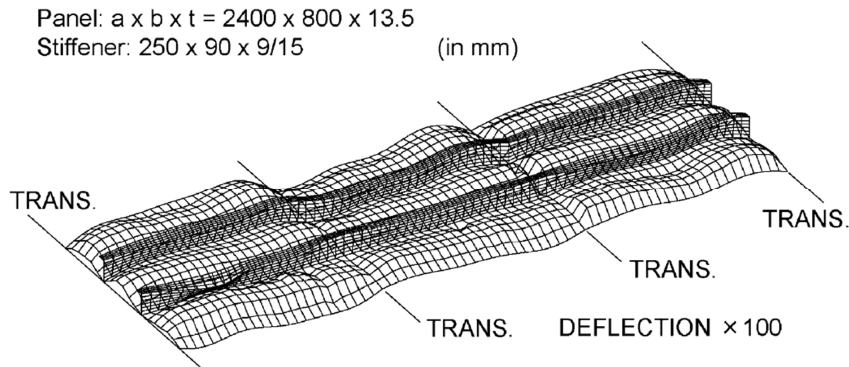


Figure 4 Real distribution of initial deflection or so-called thin-horse mode initial deflection [7, 11].

The actual mode of the initial deflection of the plate is very complex, Fig. 4 (Fujikubo et al. [6, 7]). This complex mode can be expressed by a double sinusoidal series as:

$$w_0 = \sum_{m=1}^{\infty} \sum_{n=1}^{\infty} A_{0mn} \sin \frac{m\pi x}{a} \sin \frac{n\pi y}{b} \tag{1}$$

When compressive load acts in the direction of the longer side of the plate ( $x$ -direction), the deflection components in the direction of the shorter side of the plate ( $y$ -direction) decrease

Table 1 Coefficients of thin-horse mode initial deflection as a functions of plate aspect ratio [26].

a/b	A <sub>01</sub> /t	A <sub>02</sub> /t	A <sub>03</sub> /t	A <sub>04</sub> /t	A <sub>05</sub> /t	A <sub>06</sub> /t	A <sub>07</sub> /t	A <sub>08</sub> /t	A <sub>09</sub> /t	A <sub>010</sub> /t	A <sub>011</sub> /t
$1 < a/b < \sqrt{2}$	1.1158	-0.0276	0.1377	0.0025	-0.0123	-0.0009	-0.0043	0.0008	0.0039	-0.0002	-0.0011
$\sqrt{2} < a/b < \sqrt{6}$	1.1421	-0.0457	0.2284	0.0065	0.0326	-0.0022	-0.0109	0.001	-0.0049	-0.0005	0.0027
$\sqrt{6} < a/b < \sqrt{12}$	1.1458	-0.0616	0.3079	0.0229	0.1146	-0.0065	0.0327	0.000	0.000	-0.0015	-0.0074
$\sqrt{12} < a/b < \sqrt{20}$	1.1439	-0.0677	0.3385	0.0316	0.1579	-0.0149	0.0743	0.0059	0.0293	-0.0012	0.0062
$\sqrt{20} < a/b < \sqrt{30}$	1.1271	-0.0697	0.3483	0.0375	0.1787	-0.0199	0.0995	0.0107	0.0537	-0.0051	0.0256

with the increase in load except for the first term with one half-wave. In this case, only the first term ( $n=1$ ) may play a dominant role, and the simpler form of the initial deflection can be used for the analysis as follows:

$$w_0 = \sum_{m=1}^{\infty} A_{0m1} \sin \frac{m\pi x}{a} \sin \frac{\pi y}{b} \quad (2)$$

Ueda and Yao [25] used only odd terms. Finally, Yao et al. [26] also introduced even terms into this mode, and the so-called *idealised thin-horse mode* took the following form:

$$w_0 = \sum_{m=1}^{11} A_{0m1} \sin \frac{m\pi x}{a} \sin \frac{\pi y}{b} \quad (3)$$

The initial deflection mode expressed by Eq. 3 is called *idealised thin-horse mode*, since the relevant deflection surface is similar in shape to the back of a thin horse. The coefficients of this mode are given in Table 1 (Yao et al. [26]) as functions of plate aspect ratio and its thickness. The maximum magnitude of initial deflection,  $w_{0max}$ , is taken as:

$$w_{0max} = 0.3\beta^2 t \quad (4)$$

where  $\beta$  is the slenderness parameter of the plate and defined by:

$$\beta = \frac{b}{t} \sqrt{\frac{\sigma_Y}{E}} \quad (5)$$

where  $\sigma_Y$  and  $E$  are yield stress and modulus of elasticity of the plate, respectively.

### 3.6 Validation

Nakai et al. [15] made some experiments on different pitted plates. Three of the models tested by Nakai et al. are selected in order to be simulated herein. These are identified as the models JD10, JE34 and JE56. The plate in these three models has a length of 450 mm, a width of 185 mm and a thickness of 10 mm. Diameter of the pits for the JD model is 40 mm, while in the case of the JE models is 30 mm. The two digits in the names of the models correspond to the arrangement of the pits on their surfaces. The Young's modulus of elasticity and yield strength of the material are respectively equal to 205.8 GPa and 397 MPa. Full description of the analysed models for validation purpose is given in Table 2 and Fig. 5. It has been tried to simulate numerically the tests as exactly as possible, Table 2. A comparison between the results for the ultimate strength of the models is provided in the Table 3. As can be observed,



the difference in the values of the ultimate strength of the models as obtained by FEM and test varies from 1.8 percent (in case of JD10 and JE56 models) to 8 percent (in case of JE34 model). However, it should be emphasised that many items such as the exact layout of the pits on the surfaces of the models, initial deformation mode and mesh density affects highly their responses and may lead to large variations between FEM and test results.

Table 2 Description of the analysed cases for validation purpose

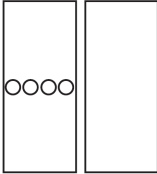
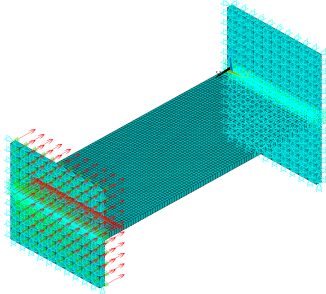
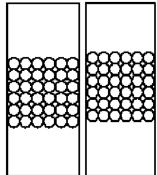
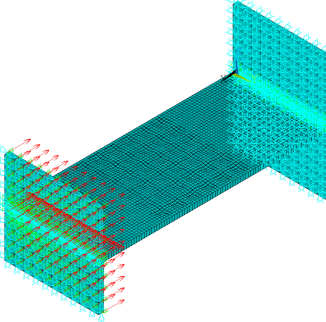
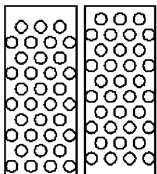
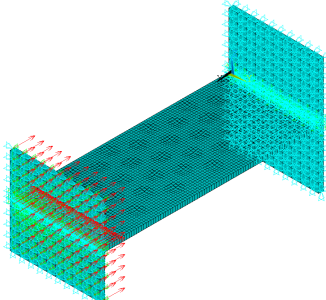
Plate 450×185 mm					
Model ID	t [mm]	Pit Distribution		Plan & B.C. View of FEM Model	t <sub>avg</sub> [mm]
		Side A	Side B		
JD10 	9.9	D1	0		9.80
		$n_{pit}=4$ $D=40$ mm $DOP=6\%$	$n_{pit}=0$ $D=0$ mm $DOP=0$		
JE34 	10.0	E3	E4		9.24
		$n_{pit}=36$ $D=30$ mm $DOP=3\%$	$n_{pit}=36$ $D=30$ mm $DOP=3\%$		
JE56 	9.9	E5	E6		9.16
		$n_{pit}=35$ $D=30$ mm $DOP=3\%$	$n_{pit}=35$ $D=30$ mm $DOP=3\%$		

Table 3 Comparison between experimental and numerical ultimate strength values for the validation models

Model ID	$(\frac{\sigma_{Ult}}{\sigma_Y})$	$(\frac{\sigma_{Ult}}{\sigma_Y})_{FEM}$	Difference (%)
JD10	0.506	0.497	-1.8
JE34	0.461	0.498	8.0
JE56	0.538	0.526	-2.2

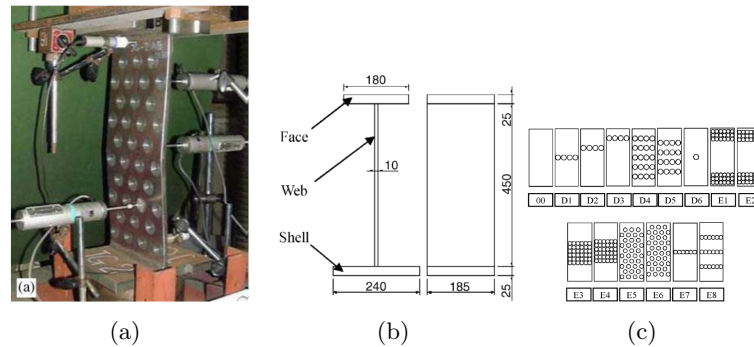


Figure 5 (a) Test rig set up with test specimen used by Nakai et al. [1], (b) An example of test specimen (all dimensions in mm), (c) Pit distribution in different specimens.

In the case of JD10 model, where the number of pits is small and pits exist only on one side of the model, the ultimate strength is strongly affected by which side is the convex of the initial deflection mode.

Besides, when the number of pits is large and they are located on both surfaces of the model, as in the cases of JE34 or JE56 models, the ultimate strength gets smaller when the pits are locally concentrated at the middle part of the model. Another important aspect in such cases is that when the pits are localised at the middle part of the model, the ultimate strength is sensitive to the shape of initial deflection mode of the model. No information on the initial deflection of the models has been reported by Nakai et al. [15]. On the other hand, the finite element simulations for these three models were performed without considering the initial deflection for them. One of the main reasons behind the 8% difference in the FEM prediction of the ultimate strength and the relevant test result in the case of JE34 model can be considered as due to neglecting the effect of initial deflection of the model in the finite element simulation.

A comparison of the experimental and numerical load-displacement relationships for the validation models is given in Table 4. It can be simply realised that the FEM results are in relatively good agreement with the test results.

Also, deformation mode and spread of plasticity at two different stress levels for the validation models as obtained by FEM are shown in Table 5. Since no information is available regarding the collapse modes of the models tested by Nakai et al. [15], the results shown in the Table 5 may be helpful in understanding the collapse mechanisms for different models.

Table 4 Comparison of experimental and numerical load-displacement relationships for the validation models

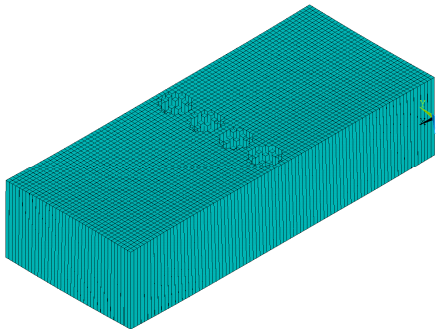
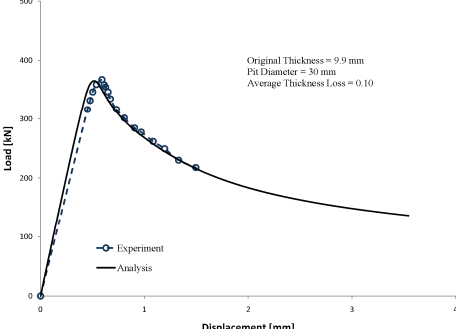
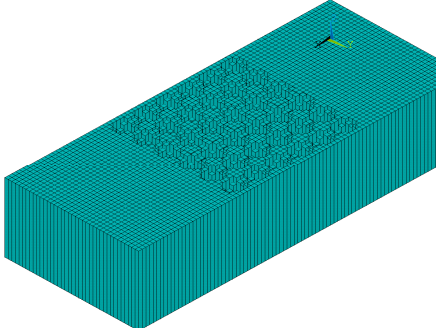
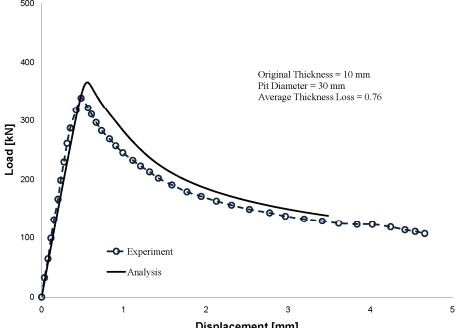
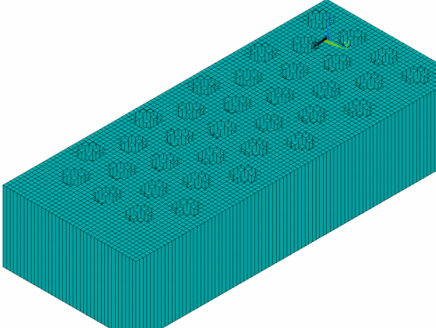
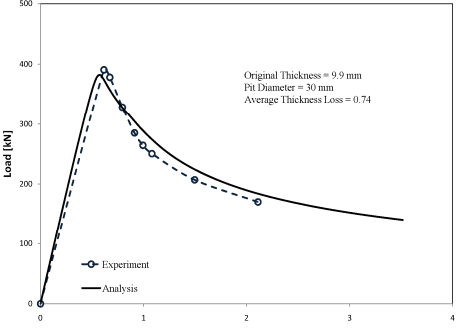
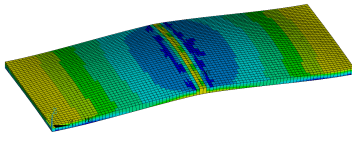
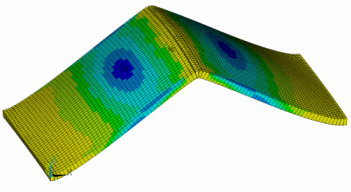
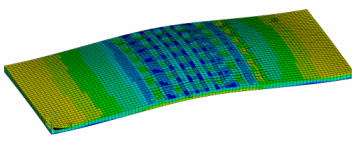
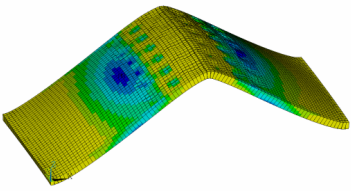
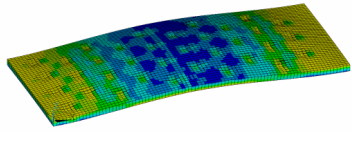
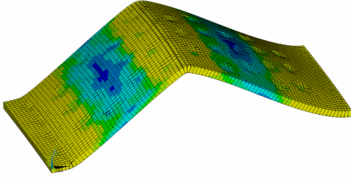

Model ID	Finite Element Model	Load-Displacement Curve
JD10		
JE34		
JE56		

Table 5 Deformation mode and spread of plasticity for the validation models as obtained by FEM (magnification factor for deformation mode: 10).

Plate 450×185 mm				
Model ID	Ultimate strength level	$\frac{\sigma_{ave}}{\sigma_y}$	Final step of calculation ( $\epsilon/\epsilon_y = 4$ )	$\frac{\sigma_{ave}}{\sigma_y}$
JD10		0.497		0.187
JE34		0.498		0.188
JE56		0.526		0.194



0    61.667    123.333    185    246.667    308.333    370    431.667    493.333    555

#### 4 PARAMETRIC STUDY

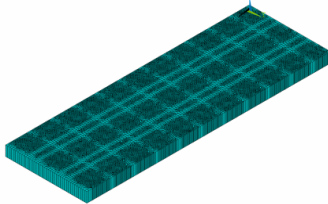
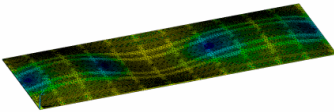
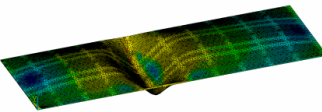
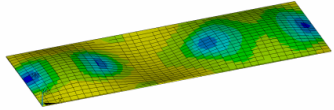
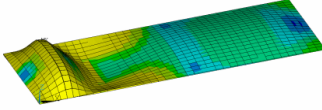
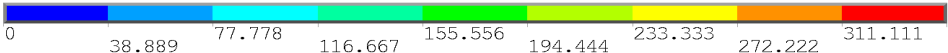
In order to study the effects of pitting corrosion on the response of axially loaded plates, different cases were considered. The cases included in the study are briefly explained as follows:

- Corroded plates with  $AR=2$ ,  $t=10$  mm,  $DOP=10\%$ ,  $20\%$ ,  $30\%$ ;  $D=20$ ,  $30$  mm;  $RDP=4$ ,  $6$ ,  $8$ ,  $10$  and made of *HTS* or *NS* steels
- Corroded plates with  $AR=3$ ,  $t=10$  mm,  $DOP=10\%$ ,  $20\%$ ,  $30\%$ ;  $D=20$ ,  $30$  mm;  $RDP=4$ ,  $6$ ,  $8$ ,  $10$  and made of *HTS* or *NS* steels
- Corroded plates with  $AR=2$ ,  $t=14$  mm,  $DOP=10\%$ ,  $20\%$ ,  $30\%$ ;  $D=20$ ,  $30$  mm;  $RDP=4$ ,  $6$ ,  $8$ ,  $10$  and made of *HTS* or *NS* steels

- Corroded plates with  $AR=3$ ,  $t=14$  mm,  $DOP=10\%$ ,  $20\%$ ,  $30\%$ ;  $D=20, 30$  mm;  $RDP=4, 6, 8, 10$  and made of *HTS* or *NS* steels
- Corroded plates with  $AR=2$ ,  $t=18$  mm,  $DOP=10\%$ ,  $20\%$ ,  $30\%$ ;  $D=20, 30$  mm;  $RDP=4, 6, 8, 10$  and made of *HTS* or *NS* steels
- Corroded plates with  $AR=3$ ,  $t=18$  mm,  $DOP=10\%$ ,  $20\%$ ,  $30\%$ ;  $D=20, 30$  mm;  $RDP=4, 6, 8, 10$  and made of *HTS* or *NS* steels

A numerical database including the characteristics of all cases and their corresponding finite element results is created in the background. Due to wide extent of the cases that were analysed in this research study, the results are shown only for some limited cases. Deformation mode and spread of plasticity for some pitted plates are shown in Tables 6, 7, 8 and 9 for two different strength levels. Also, average stress-average strain relationship for those pitted plates is represented by solid line in Figures 6, 7, 8 and 9. The number of half-waves in the ultimate strength modes of the plates is equal to the aspect ratio of the plates. It can be seen that the half-waves in the ultimate strength mode of the pitted plates are of regular form.

Table 6 Deformation mode and spread of plasticity for the plate of dimensions  $2400 \times 800$  mm ( $AR=3$ ),  $D=20$  mm,  $DOP=20\%$ ,  $RDP=4$ , made of NS Steel (magnification factor for deformation mode: 10).

Case	Ultimate strength level	Final step
 Pitted $AR=3$ , $t=10$ mm, $t_{eq}=8.5$ mm, NS		
Uniformly Corroded $AR=3$ , $t=8.5$ mm, NS		
		

Elastic buckling occurs in case of some slender plates as shown in Figs. 6 and 7. As a combined effect of local accumulation of plastic deformation and also unloading in the plate models, load shedding is appeared in the post-ultimate-strength regions of the average stress-average strain relationships. The place of local accumulation of plastic deformation can be either at the end sub-panels or middle sub-panels of the plate models, depending on their aspect ratio and corrosion characteristics.

Table 7 Deformation mode and spread of plasticity for the plate of dimensions 2400×800 mm ( $AR=3$ ),  $D=20$  mm,  $DOP=30\%$ ,  $RDP=4$ , made of HTS Steel (magnification factor for deformation mode: 10).

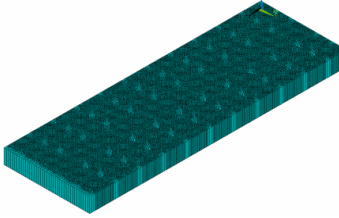
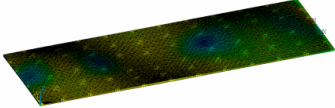
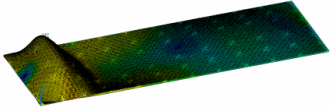
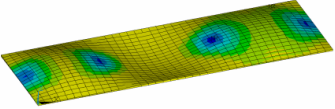
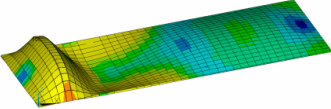
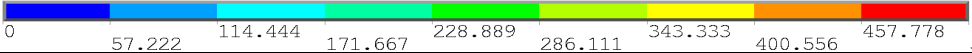
Case	Ultimate strength level	Final step
 <p>Pitted  <math>AR=3</math>, <math>t=14</math> mm, <math>t_{eq}=12.0</math> mm,                      HTS</p>		
<p>Uniformly Corroded  <math>AR=3</math>, <math>t=12.0</math> mm, HTS</p>		
 <p>0    57.222    114.444    171.667    228.889    286.111    343.333    400.556    457.778    515</p>		

Table 8 Deformation mode and spread of plasticity for the plate of dimensions 2400×800 mm ( $AR=3$ ),  $D=30$  mm,  $DOP=10\%$ ,  $RDP=6$ , made of NS Steel (magnification factor for deformation mode: 10).

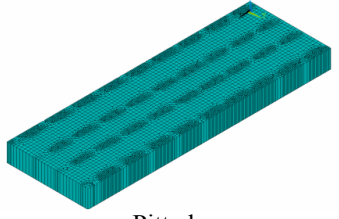
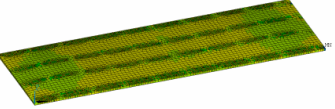
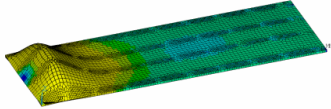
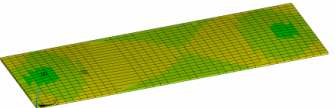
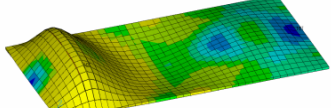

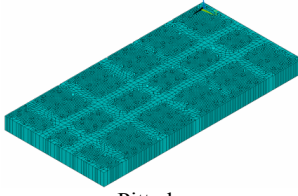
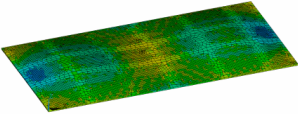
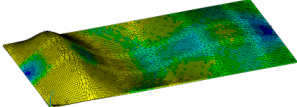
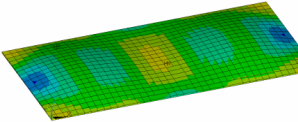
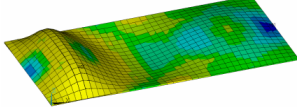

Case	Ultimate strength level	Final step
 <p>Pitted  <math>AR=3</math>, <math>t=18</math> mm, <math>t_{eq}=17.0</math> mm,                      NS</p>		
<p>Uniformly Corroded  <math>AR=3</math>, <math>t=17.0</math> mm, NS</p>		
 <p>0    38.889    77.778    116.667    155.556    194.444    233.333    272.222    311.111    350</p>		

Table 9 Deformation mode and spread of plasticity for the plate of dimensions 1600×800 mm ( $AR=2$ ),  $D=30$  mm,  $DOP=20\%$ ,  $RDP=10$ , made of NS Steel (magnification factor for deformation mode: 10).

Case	Ultimate strength level	Final step
 Pitted $AR=2$ , $t=10$ mm, $t_{eq}=9.5$ mm, NS		
Uniformly Corroded $AR=2$ , $t=9.5$ mm, NS		
		

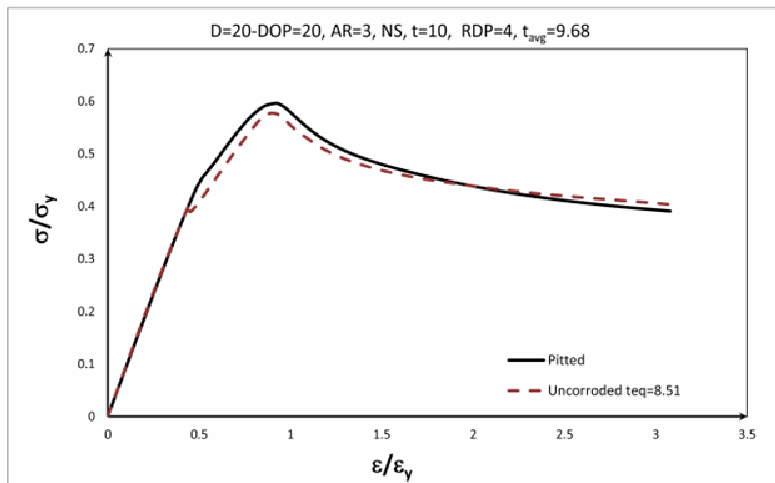


Figure 6 Comparison of average stress-average strain relationships for a pitted plate (with  $AR=3$ ,  $t=10$  mm,  $D=20$  mm,  $DOP=20\%$ ,  $RDP=4$ ,  $t_{avg}=9.68$  mm,) and its equivalent uniformly corroded plate (with  $AR=3$ ,  $t_{eq}=8.51$  mm) made of NS steel.

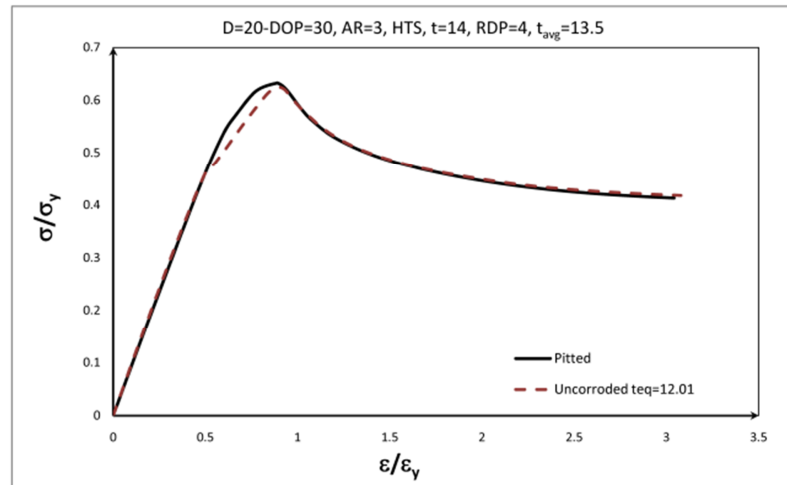


Figure 7 Comparison of average stress-average strain relationships for a pitted plate (with AR=3, t=14 mm, D=20 mm, DOP=30%, RDP=4, t<sub>avg</sub>=13.5 mm,) and its equivalent uniformly corroded plate (with AR=3, t<sub>eq</sub>=12.01 mm) made of HTS steel.

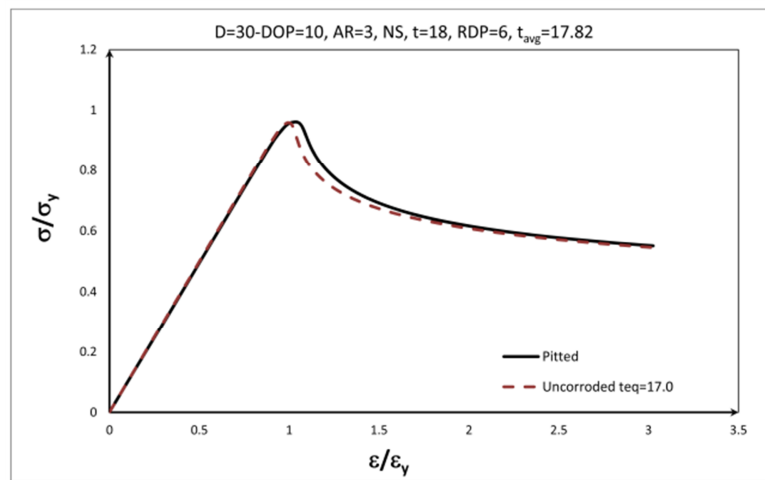


Figure 8 Comparison of average stress-average strain relationships for a pitted plate (with AR=3, t=18 mm, D=30 mm, DOP=10%, RDP=6, t<sub>avg</sub>=17.82 mm,) and its equivalent uniformly corroded plate (with AR=3, t<sub>eq</sub>=17.0 mm) made of NS steel.



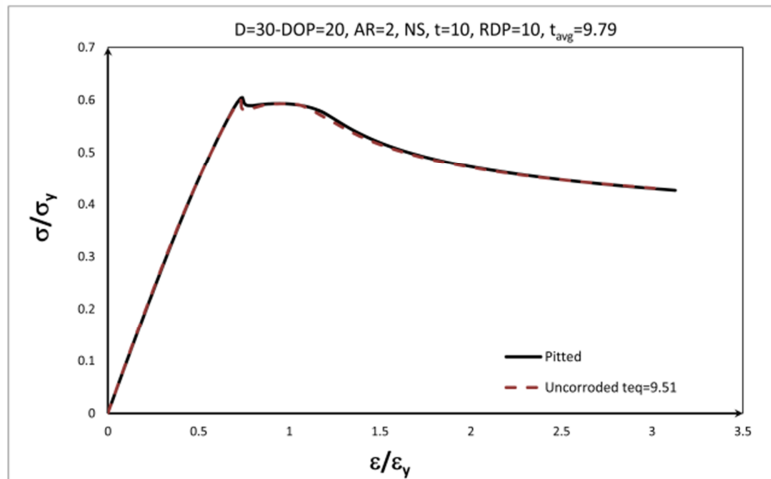


Figure 9 Comparison of average stress-average strain relationships for a pitted plate (with AR=2, t=10 mm, D=30 mm, DOP=20%, RDP=10, tavg=9.79 mm,) and its equivalent uniformly corroded plate (with AR=2, teq=9.51 mm) made of NS steel.

### 5 PROPOSAL ON EFFECTIVE THICKNESS

In order to reach an effective thickness proposal, first a series of elastic-plastic large deflection finite element analyses is performed on the uncorroded plates under longitudinal compression. The thickness of the plates ranges from 7.5 mm to 19 mm. The values of the ultimate strength and final strength (at  $\epsilon/\epsilon_Y = 3$ ) are extracted out of the finite element analyses. These strength values are then normalised or nondimensionalised by  $\sigma_Y$ , Fig. 10. Based on the results in Fig. 10, the following equations can be derived

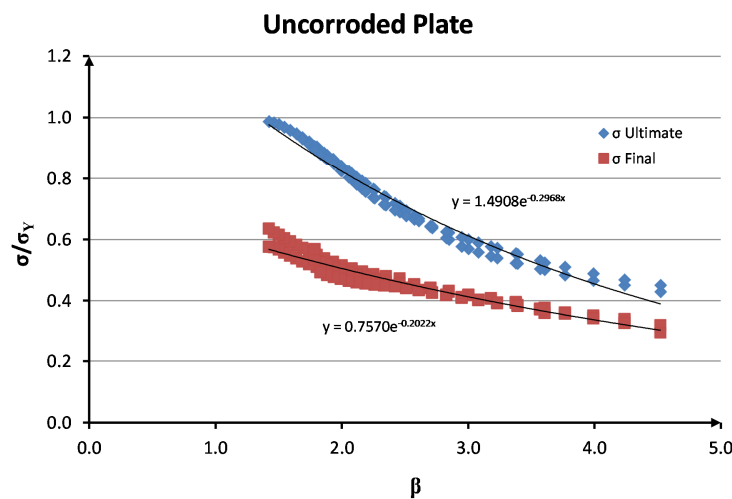


Figure 10 The relationship between strength values normalised by the value of yield strength and slenderness ratio for uncorroded plate.

$$\sigma_{Ult}/\sigma_Y = 1.4908e^{-0.2968\beta} \tag{6}$$

$$\sigma_{Final}/\sigma_Y = 0.7570e^{-0.2022\beta} \tag{7}$$

On the other hand, the following formulation can be written for a pitted plate

$$V_{corroded} = n_{pit} \cdot V_{pit} \tag{8}$$

and

$$t_{avg} = \frac{V_{uncorroded} - V_{corroded}}{A} \tag{9}$$

where  $t_{avg}$  represents the average thickness of the pitted plate based on the volume of the pits. The value of  $t_{avg}$  is calculated for each case and registered within the database of analyses.

In order to reach a preliminary formulation for the value of the equivalent thickness of the pitted plate, two conditions are considered to be fulfilled here. The first condition describes that the ultimate strength of the pitted plate is to be equal to the ultimate strength of the uncorroded plate given by Eq. (6). And also the other condition is equality of the final strength of the pitted plate with the final strength of the uncorroded plate given by Eq. (7). For each case of the analysed pitted plates in the database of the current research study, these two conditions are used in order to obtain the nearest possible value of the thickness for an uncorroded plate yielding approximately the same values of the strengths as the pitted plate. These values of the equivalent thicknesses are registered in the database. Figure 11 demonstrates the relationship between the values of  $t_{eq}$  and  $t_{avg}$ , which can be easily formulated as

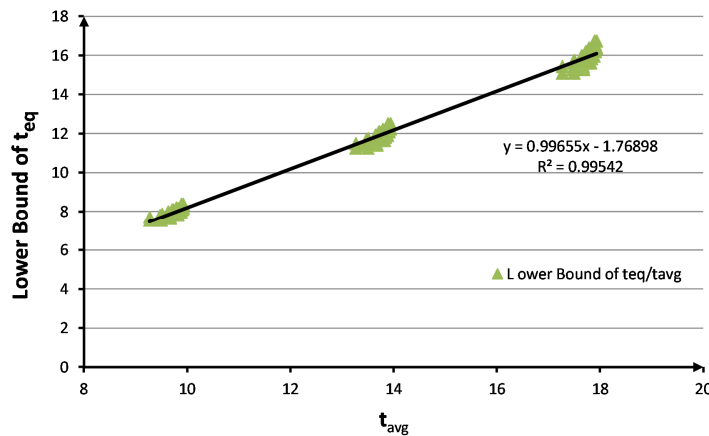


Figure 11 The relationship between strength values normalised by the value of yield strength and slenderness ratio for uncorroded plate.

$$t_{eq} = 0.99655t_{avg} - 1.76898 \tag{10}$$

In a trial and error attempt and based on the developed database of the pitted plates, a coefficient  $\alpha$  is defined as below in order to establish a relationship between different parameters describing the status of any pitted plate

$$\alpha = t^{1.11} \left[ \frac{\left(\frac{D_{pit}}{H_{pit}}\right)^{0.05}}{AR^{0.05} DOP^{0.03}} \right] \tag{11}$$

The parameters and their powers included in the Eq. (11) are so adopted that a relationship between the coefficient  $\alpha$  and effective thickness  $t_{eq}$  can be extracted. Obtaining the values of  $\alpha$  for each case within the database, the following relationship can be easily written

$$t_{eq} = 0.697\alpha + 0.47 \tag{12}$$

The relationship between the values of  $t_{eq}$  and  $\alpha$  is shown in Fig. 12 from which the following lower bound value for the  $t_{eq}$  can be obtained

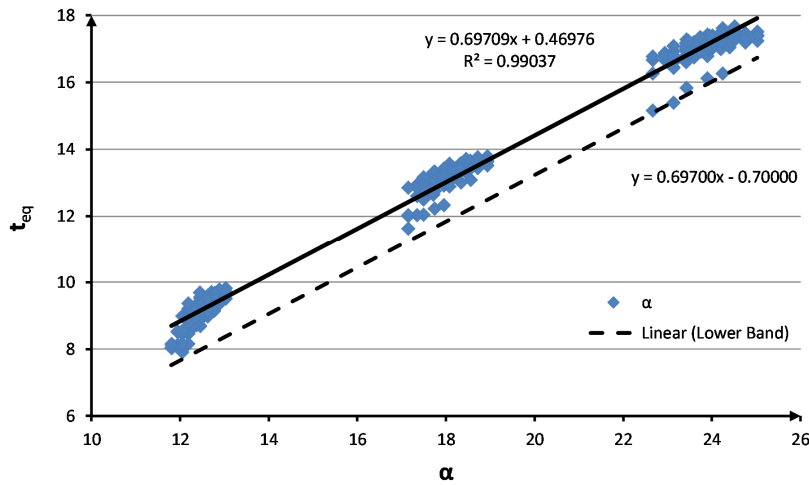


Figure 12 The relationship between the values of  $\alpha$  and  $t_{eq}$ .

$$t_{eq}(lower\ Bound) = 0.697\alpha - 0.7 \tag{13}$$

Eqs. (12) or (13) can be used in order to obtain estimates of the equivalent thickness for a pitted plate. Besides, as an alternative way to do this, the value of equivalent mean corrosion depth of the pitted plate ( $\mu$ ) is determined as

$$\mu = t - t_{avg} \tag{14}$$

Figure 13 shows the scatter of the values for  $\mu$ , based on which the following relationship can be obtained in order to give an estimate of the effective thickness of the pitted plate

$$t_{eq}(lowerbound) = t - \mu(upperbound) \tag{15}$$

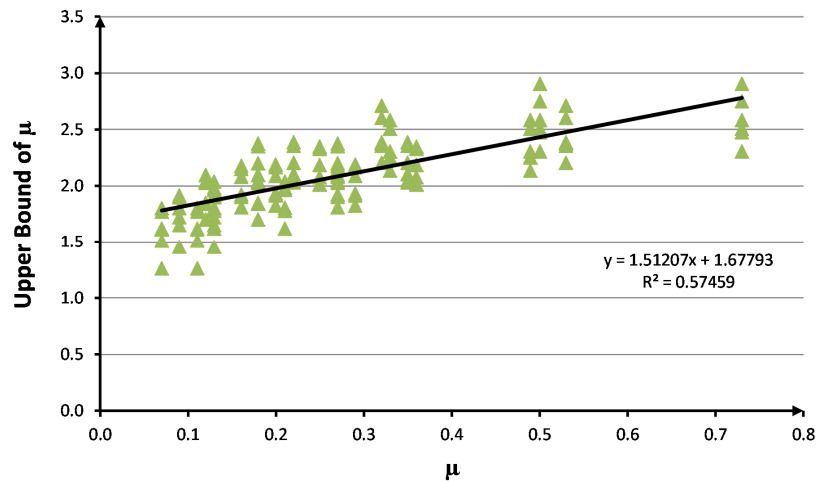


Figure 13 The relationship between the upper bound value of and.

where

$$\mu(\text{upper bound}) = 1.51207\mu + 1.67793 \quad (16)$$

For each case of the pitted plates in Tables 6 to 9, the results for the equivalent uniformly corroded plates are also shown. There is a high degree of coincidence among the results for any of the pitted plates and its corresponding equivalent uniformly corroded plate. Also, a comparison between the average stress-average strain relationships for the pitted plates and their corresponding equivalent uniformly corroded plates is given in Figs. 6 to 9, for some limited cases. A very good agreement is demonstrated among them. This reveals the usefulness of the proposed equations for estimation of the equivalent thickness of the pitted plates.

## 6 CONCLUSIONS

Some available tested models suffering pitting corrosion are numerically simulated first. The results show good capability of the software and numerical model in order to establish a framework for studying the response of the pitted plates. Based on the gathered experience, series of validated nonlinear elastic-plastic finite element analyses have been performed on the plates in different un-corroded and pitted conditions. The plates have been subjected to in-plane compression load. Full-range average stress-average strain relationships of the plates have been derived considering the changes in plate aspect ratio, plate slenderness or thickness, density of pitting, pit diameter and ratio of pit diameter to the depth of the pits. A database of the analysed cases is created. Different characteristics of the response of the pitted plates to the in-plane compression are briefly discussed. In order to investigate the strength characteristics of the pitted plate under the longitudinal in-plane compression without any modelling of the pitting, a practical proposal was developed to calculate the effective thickness of the plate. The proposed effective thickness formulation for the pitted plates can be easily implemented

in the strength analysis procedures of plated structures suffering pitting corrosion. This can be achieved through replacement of the pitted plates with their equivalent uncorroded plates.

Although emphasize was concentrated on the in-plane uni-axial compressive loading of the pitted plates in this study, investigation of their behaviours under other types of the loads remains as future works.

## References

- [1] Asm international corrosion. asm handbook. 13, 2001.
- [2] Ansys 11.0 reference manual, ansys inc., 2008.
- [3] H.K.K. Amlashi and T. Moan. On the strength assessment of pitted stiffened plates under biaxial compression loading. In *In: 24th international conference on offshore mechanics and arctic engineering*, Halkidiki, Greece, 2005.
- [4] J.C. Daidola, J. Parente, I.R. Orisamolu, and K.T. Ma. Residual strength assessment of pitted plate panels. 1997.
- [5] S. Saad Eldeen and C. Guedes Soares. Effect of pitting corrosion on the collapse strength of rectangular plates under axial compression. In *Proceedings of Analysis and Design of Marine Structures*, pages 231–236, Portugal, 2009.
- [6] M. Fujikubo, S. Harada, T. Yao, M.R. Khedmati, and D. Yanagihara. Estimation of ultimate strength of continuous stiffened panel under combined transverse thrust and lateral pressure, part 2: Continuous stiffened panel. *Marine Structures*, 18:411417, 2005.
- [7] M. Fujikubo, T. Yao, M.R. Khedmati, S. Harada, and D. Yanagihara. Estimation of ultimate strength of continuous stiffened panel under combined transverse thrust and lateral pressure, part 1: Continuous plate. *Marine Structures*, 18:383410, 2005.
- [8] Y. Huang, Y. Zhang, G. Liu, and Q. Zhang. Ultimate strength assessment of hull structural plate with pitting corrosion damnification under biaxial compression. *Ultimate Strength of Plates with Random Fields of Corrosion*, 4:363–370, 2008.
- [9] Y. Huang, Y. Zhang, G. Liu, and Q. Zhang. Ultimate strength assessment of hull structural plate with pitting corrosion damnification under biaxial compression. *Ocean Eng*, 13:1503–1512, 2010.
- [10] X. Jiang and C. Guedes Soares. Ultimate compressive capacity of mild steel plates with single and double side corrosion pits. In *Proceedings of the TEAM 2009*, Kaohsiung, Taiwan, 30 November-3 December 2009.
- [11] M.R. Khedmati. *Ultimate strength of ship structural members and systems considering local pressure loads*. PhD thesis, Graduate School of Engineering, Hiroshima University, September 2000.
- [12] M.R. Khedmati, Z.H.M.E. Nouri, and M.M. Roshanali. An effective thickness proposal for strength evaluation of both-sides randomly corroded steel plates under uniaxial compression. *Steel and Composite Structures*. Accepted for Publication.
- [13] M.R. Khedmati, Z.H.M.E. Nouri, and M.M. Roshanali. Strength of steel plates with both-sides randomly distributed with corrosion wastage under uniaxial compression. *Thin Walled Struct*, 49(2):325342, 2011.
- [14] A.F. Mateus and J.A. Witz. On the buckling and post-buckling of corroded steel plates. 1998.
- [15] T. Nakai, H. Matsushita, and N. Yamamoto. Effect of pitting corrosion on local strength of hold frames of bulk carriers (1st report). *Mar Struct*, 17:403–432, 2004.
- [16] T. Nakai, H. Matsushita, and N. Yamamoto. Effect of pitting corrosion on local strength of hold frames of bulk carriers (2nd report) lateraldistortional buckling and local face buckling. *Mar Struct*, 17:612641, 2004.
- [17] Z.H.M.E. Nouri, M.R. Khedmati, and M.M. Roshanali. Degradation of the compressive strength of unstiffened/stiffened steel plates due to both-sides randomly distributed corrosion wastage. *Latin American Journal of Solids and Structures*, 7(3):335–367, 2010.
- [18] D. Ok, Y. Pu, and A. Incecik. Computation of ultimate strength of locally corroded unstiffened plates under uniaxial compression. *Mar Struct*, 20:100114, 2007.
- [19] J.K. Paik, J.M. Lee, and M.J. Ko. Ultimate compressive strength of plate elements with pit corrosion wastage. *J Eng Mar Environ*, 217.

- [20] J.K. Paik, J.M. Lee, and M.J. Ko. Ultimate shear strength of plate elements with pit corrosion wastage. *Thin Walled Struct*, 42:11611176, 2004.
- [21] J.K. Seo, B.J. Kim, H.S. Ryu, Y.C. Ha, and J.K. Paik. Validation of the equivalent plate thickness approach for ultimate strength analysis of stiffened panels with non-uniform plate thickness. *Thin Walled Struct*, 49:753–761, 2011.
- [22] Dunbar TE and et al. A computational investigation of the effects of localized corrosion on plates and stiffened panels. *Mar Struct*, 17(5):385402, 2004.
- [23] A.P. Teixeira and C. Guedes Soares. Probabilistic modelling of the collapse behaviour of plates with random corrosion fields. In *Proceedings of the 2005 Conference on Numerical Methods in Engineering*, pages 4–7, Granada, Spain, SEMNI, July 2005.
- [24] A.P. Teixeira and C. Guedes Soares. Probabilistic modelling of the ultimate strength of plates with random fields of corrosion. In *Proceedings of the 5th Computational Stochastic Mechanics Conference (5CSM)*, pages 21–23, Rhodes-Greece, June 2006.
- [25] Y. Ueda and T. Yao. The influence of complex initial deflection on the behaviour and ultimate strength of rectangular plates in compression. *J. of Const. Steel Research*, 5:265–302, 1985.
- [26] T. Yao, P.I. Nikolov, and Y. Miyagawa. Influence of welding imperfections on stiffness of rectangular plates under thrust. In K. Karlsson, L.E. Lindgren, and M. Jonsson, editors, *Proc. of IUTAM Sump. on Mechanical Effects of Welding*, pages 261–268. Springer-Verlag, 1992.
- [27] Y. Zhang, Y. Huang, and G. Liu. A study on assessment of ultimate strength of ship structural plate with pitting corrosion damnification. In *Proceedings of the Eighth ISOPE Pacific/Asia Offshore Mechanics Symposium*, pages 10–14, Bangkok, Thailand, November 2008.